

## Eco-friendly synthesis of *Solanum trilobatum* extract-capped silver nanoparticles is compatible with good antimicrobial activities

Santheraleka Ramanathan<sup>a</sup>, Subash C.B. Gopinath<sup>a, b, \*</sup>, Periasamy Anbu<sup>c, \*\*</sup>,  
Thangavel Lakshmipriya<sup>d</sup>, Farizul Hafiz Kasim<sup>a, e</sup>, Choul-Gyun Lee<sup>c</sup>

<sup>a</sup> School of Bioprocess Engineering, University Malaysia Perlis, 02600 Arau, Perlis, Malaysia

<sup>b</sup> Institute of Nano Electronic Engineering, University Malaysia Perlis, 01000 Kangar, Perlis, Malaysia

<sup>c</sup> Department of Biological Engineering, College of Engineering, Inha University, Incheon 402-751, Republic of Korea

<sup>d</sup> Centre of Innovative Nanostructure & Nanodevices, Universiti Teknologi PETRONAS, 32610 Bandar Seri Iskandar, Perak Darul Ridzuan, Malaysia

<sup>e</sup> Centre of Excellence for Biomass Utilization, School of Bioprocess Engineering, Universiti Malaysia Perlis, 02600 Arau, Perlis, Malaysia

### ARTICLE INFO

#### Article history:

Received 13 December 2017

Received in revised form

20 January 2018

Accepted 21 January 2018

Available online 5 February 2018

#### Keywords:

Silver nanoparticle

Green synthesis

*Solanum trilobatum*

Antimicrobial activity

Medicinal plant

### ABSTRACT

This study focused on the evaluation of antimicrobial activity of silver nanoparticles (AgNPs) after their green synthesis by means of a *Solanum trilobatum* bark extract. The obtained product with an intense surface plasmon resonance band at ~442 nm with UV–visible spectroscopic analysis indicated the formation of AgNPs. The morphology of AgNPs was observed under transmission electron microscopy and field emission scanning electron microscopy, displayed that the eco-friendly synthesized AgNPs have a spherical shape with an average size of ~25 nm in diameter. X-ray powder diffraction and selected area electron diffraction analyses confirmed that the AgNPs are crystalline in nature. Fourier transform infrared spectroscopy indicated that the AgNPs capped with active ingredients of the bark extract. X-ray photoelectron spectroscopy revealed elemental composition of the AgNPs. The performance of *S. trilobatum* bark extract-capped AgNPs in terms of inhibition of microbial growth was studied by disc diffusion and well diffusion assays. Eco-friendly synthesized *S. trilobatum* extract-capped AgNPs were found to possess enhanced antimicrobial properties: growth inhibition of gram-negative and gram-positive bacteria and of fungal species. These results demonstrated the potential applications of the indigenous medicinal plants to the field of nanotechnology.

© 2018 Elsevier B.V. All rights reserved.

### 1. Introduction

Norio Taniguchi from Tokyo Science University first proposed the term nanotechnology in 1974. On the other hand, Richard Feynman, an American theoretical physicist has initiated the concept of manufacturing small scale and he stated that if cell capabilities as micro-building blocks, are good enough for assembling littler things on a nuclear level. The innovation among scientists in the research on the manufacture of atomic-size components has resulted in the invention of nanotechnology. Since then, nanotechnology has been implemented in various fields with a big

impact according to the data on recent expenditures in this field [1]. Nanotechnology has been broadly applied for the development of therapeutics, electronics, environmentally friendly energy, and to other commercial industries.

The relevant branches of science and engineering have shown that nanoparticles produced from bulk material alone are less effective. The conjugation of reducing agent with metals is increasingly used for the production of metallic nanoparticles. Among various metals in this industry, silver is a major element used in nanoparticles. Silver nanoparticles (AgNPs) serve as a coating for devices, microelements of electronics and optoelectronics, and construction materials in buildings, along with many other daily uses. Nevertheless, healthcare and medical fields use silver in almost all nanoparticle-related services and applications. The anti-infective properties of AgNPs are the main reason for the wide range of their applications in various fields [2]. AgNPs are known to be a generic medication. The properties of AgNPs against infections broaden their use in drugs, treatment methods, and

\* Corresponding author. School of Bioprocess Engineering, University Malaysia Perlis, 02600 Arau, Perlis, Malaysia.

\*\* Corresponding author.

E-mail addresses: [subash@unimap.edu.my](mailto:subash@unimap.edu.my) (S.C.B. Gopinath), [anbu25@inha.ac.kr](mailto:anbu25@inha.ac.kr) (P. Anbu).

medical devices. AgNPs mimic the function of some medicines by alleviating several human illnesses, thus proving that AgNPs can serve as a generic medication.

Several methods have been used to synthesize the AgNPs. The physical method of synthesis of AgNPs is better than the chemical method in terms of solvent contamination of nanoparticles. However, the large tube furnace for particle evaporation and condensation requires lots of energy. Moreover, the significance of maintaining the parameters in the tube furnace such as extremely high and low temperature and pressure regulators require much time for completion of AgNP synthesis, and this approach was found to be costly for the overall process. In the chemical method, reducing agents, protective agents, and surfactants are used to prevent particle aggregation and to synthesize highly stable nanoparticles. Contamination of nanoparticles occurs when many chemicals are consumed during nanoparticle synthesis. The use of strong reducing agents in the chemical synthesis of AgNPs results in a larger size of AgNPs, and it is difficult to control the size variations. In contrast, a weak reducing agent such as citrate generates monodisperse AgNPs (narrow size range); however, the time necessary to complete the AgNP synthesis is longer than usual. To overcome these complications, two-stage chemical reduction of AgNPs was proposed, which uses a strong reducing agent at first, followed by the weak one as a capping agent. With this reduction strategy, stable AgNPs with less variation in size and shape are generated. Nonetheless, the use of two chemical agents in a process can lead to the synthesis of hazardous AgNPs contaminated with a solvent. Alternatively, green synthesis was found to be a cost-effective and environmentally friendly method of synthesis to obtain stable AgNPs, and is superior to other methods of synthesis owing to its potential for synthesizing AgNPs by means of only bio-based reducing and capping agents [3]. The optimal conditions for eco-friendly synthesis of AgNP are well established; consequently, they can be applied to a large-scale AgNP synthesis. Green synthesis of AgNPs is simple and known as a one-step process that can generate stable nanoparticles [4].

*Solanum trilobatum*, commonly known as purple-fruited pea eggplant, originates from India. It also grows in southern regions of Asia, in Myanmar, Vietnam, Thailand, and Malaysia. This herb can easily grow on land and in a climate of India as well as in Asia, which is more suitable for cultivation of the plant and fruits of *S. trilobatum*. *S. trilobatum* falls into the category of medicinal plants because it contains various types of bioactive substances, which make it useful for health care. The stem, leaves, fruits, and seeds of the herb contain solasoline. The latter of the plant is a type of steroid that has been utilized in the production of steroid drugs. Originally, the herb was used as the primary home remedy for certain illnesses in India, and it is still used by rural residents. The herb is also used as a home remedy to treat asthma, respiratory problems, cough, gastric disorders, gas in the digestive tract, and constipation. The ability of this herb to cure all these illnesses proves that it is highly resistant to any type of infection and diseases. Besides its use as a home remedy, *S. trilobatum* has proven to possess antibacterial, antifungal, antioxidant, and antitumor effects based on the bioactive substances in this herb. The herb also has hepatoprotective properties, which protect the liver from UV irradiation. Research has shown that the herb also has an anti-ulcerogenic activity according to experiments with a bacterial attack on the postlarval stage of *Penaeus monodon* [5]. AgNPs synthesized from unripe fruits of *S. trilobatum* were shown to have anti-cancer activity *in vitro*, in which these nanoparticles were proved with an inhibition against human breast cancer cell line (MCF-7), demonstrated by MTT assay, nuclear morphology assay, Western blot and RT-PCR analyses [6]. Moreover, the leaf extract of *S. trilobatum* was proved to have antimicrobial property against the

bacterial strains, such as *Bacillus subtilis*, *Staphylococcus aureus*, *B. cereus*, *E. coli* and *Pseudomonas aeruginosa* [7].

Due to the above-mentioned positive medicinal properties of *S. trilobatum*, it is worthwhile to prepare AgNPs by means of this herb's extract using a conventional method for green synthesis. Previously, preparation of AgNPs with plants such as *Camellia sinensis*, *Ocimum sanctum*, and *Datura metel* was studied for the antimicrobial properties and further transformation of these nanoparticles has been used in the manufacture of medicines. As such, incorporation of ingredients of *S. trilobatum* bark extract into AgNP can be performed to study the antimicrobial activities and the potential for the development of pharmaceutical products. In this study, green synthesis of AgNP was accomplished by using an *S. trilobatum* bark extract as a reducing agent. In addition, characterization of *S. trilobatum* ingredients incorporated AgNPs was further performed for the enhanced antimicrobial activities.

## 2. Materials and methods

### 2.1. Collection and preparation of *S. trilobatum* bark extract

*S. trilobatum* was collected in Tamil Nadu, India. The bark of the plant was separated from the whole herb and cut into small pieces; 5 g of bark was cleaned and weighed for bark extract preparation. The bark was washed with 100 mL of 0.05% Tween 20 detergent and the solution was discarded. Washing process was continued with double-distilled water, where 100 mL of sterile distilled water was added to the 5 g of bark for washing. This step was repeated two times to ensure that the dirt and impurities from the bark were removed. To prepare the bark extract, the dried bark was placed into a beaker which contained 50 mL of sterile distilled water. The beaker was then covered with aluminum foil and stored in a closed area overnight. On the next day, the mixture was boiled at 55 °C for 10 min using a hot plate stirrer. After boiling, the solution was left to cool down before the extraction process. A strainer was used to filter the bark extract solution and remove the bark together with other suspended particles. The filtered solution was then filtered again using a 0.45- $\mu\text{m}$  microfilter to obtain an uncontaminated bark extract solution. The bark extract was kept at 4 °C for AgNP synthesis.

### 2.2. Culturing microorganisms on selective agar

The strains of *Escherichia coli*, *Bacillus* sp., and *Aspergillus niger* were obtained from a microorganism stock collection at the School of Bioprocess Engineering, University of Malaysia Perlis. A microbial strain that was obtained from the stock was streaked on selective agar. The grown culture was used for the preparation of an inoculum using enrichment broth. For the preparation of the bacterial inoculum, the nutrient broth was used as the enrichment medium. For the preparation of the inoculum, two loops of a culture bacterium were inoculated into 100 mL of sterilized nutrient broth. The suspension was then placed for incubation in an incubator shaker overnight at 37 °C. There was no suspension prepared for *A. niger* because the determination of antimicrobial activity of fungi is conducted by means of a pinpoint inoculum. Spreading on a plate was used in order for the culture to grow on a selective agar plate, which was then used for the antimicrobial assay of AgNPs. Table S1 shows the different types of media used for agar plate preparation for the bacteria and fungi used in the experiments.

There are few differences in the preparation of agar plates for disc diffusion and well diffusion assay. The initial step for the disc diffusion assay is to the culture of *E. coli* and *Bacillus* sp. in a selective agar plate: 100  $\mu\text{L}$  of a bacterial suspension was added into a nutrient agar (NA) plate. The suspension was equally spread on the

agar plate using a glass spreader. Next, approximately four sterilized disk-shaped filters were placed on the test organism agar plate. The active ingredient that has an antimicrobial property was added to each disc filter, and all the experiments were conducted with a volume adjusted to 50  $\mu\text{L}$ . The plates were incubated for 24 h at 37 °C. The zone of inhibition surrounding the disc revealed the antimicrobial activity of the bark extract solution. The diameter of the zone of inhibition in millimeters was measured.

The well-diffusion assay is similar to the disc diffusion assay: the agar plate was inoculated with bacterial suspension by the method of spreading on a plate. Next, a well or hole ~6–8 mm in size was created on the agar plate. The wells were made of perfectly the same size on the bacteria-inoculated agar plate. Then, the active ingredient with an antimicrobial property was added to each well, and the volume was adjusted to 100  $\mu\text{L}$ ; a similar volume was used throughout the experiments. The plates were incubated for 24 h at 37 °C in an incubator, and the zone of inhibition of microbial growth was measured as a diameter.

As mentioned above, *A. niger* does not require inoculum suspension preparation because the antimicrobial analysis of fungi was performed by means of a pinpoint inoculum. In this case, PDA plates were prepared with a sterilized disc filter and wells for disc diffusion and a well-diffusion assay, respectively, and the active ingredients were added to the plates accordingly. Next, an inoculum of *A. niger* culture was patted lightly at the center of the PDA agar plate. The plates were incubated for 48 h at 37 °C. Then, the zone of inhibition of fungal growth was examined, and the distance of fungal inhibition from the inoculation point to the disc or well was analyzed.

### 2.3. Antimicrobial activity of the bark extract

#### 2.3.1. Serial dilution of the bark extract

To study the antimicrobial activity of the *S. trilobatum* bark extract, a serial dilution was performed for the bark extract. Five Eppendorf tubes were prepared and labeled 1, 2, 3, 4, and 5. Next, 100  $\mu\text{L}$  (100%) of the bark extract solution was pipetted into tube 1 using a micropipette. In order to perform the serial dilution, 50  $\mu\text{L}$  (50%) of the solution from tube 1 was pipetted into tube 2 and these steps were repeated until the dilution of 6.3%. The weight per volume of the bark extract solution in each tube was calculated and decreased from tube 1 to tube 5 as 5  $\mu\text{g}$  per 50  $\mu\text{L}$ , 2.5  $\mu\text{g}$  per 50  $\mu\text{L}$ , 1.25  $\mu\text{g}$  per 50  $\mu\text{L}$ , 0.625  $\mu\text{g}$  per 50  $\mu\text{L}$ , to 0.3125  $\mu\text{g}$  per 50  $\mu\text{L}$ , respectively.

#### 2.3.2. Determination of antimicrobial activity of the bark extract

For the disc diffusion assay, the bark extract that was serially diluted was added to each disc filter at 50  $\mu\text{L}$  from tube 1 to tube 5. The plates were incubated for 24 h at 37 °C in an incubator. The zone of inhibition surrounding the disc indicated the antimicrobial activity of the bark extract. The lowest amount of bark extract needed to observe the zone of inhibition of microbial activities in agar plates is known as the minimum inhibitory concentration (MIC). MIC was calculated to evaluate the optimal amount of bark extract required to inhibit the microbe. Water was added to a filter paper as a negative control. A positive control plate was prepared using ampicillin as the inhibiting agent. The zone of inhibition by ampicillin was tested by varying the amount of ampicillin added onto a filter disc. Thus, a 1 mg/mL ampicillin stock solution was prepared for serial dilution as the active ingredient against *E. coli*, *Bacillus* sp., and *A. niger*. The serial dilution for ampicillin was performed in the same way as for the bark extract solution during the determination of antimicrobial activity. The experiments were carried out in triplicate for statistical analysis.

The well-diffusion assay was performed similarly to the disc

diffusion assay: the bark extract was added to the each well at 100  $\mu\text{L}$  from tube 1 to tube 5. The plates were incubated for 24 h at 37 °C in an incubator. The tests were carried out in triplicate for each species of microorganism. It was expected that the antimicrobial component diffuses through the agar and inhibits the growth of a microorganism. The vital amount of AgNP for microbial inhibition in an agar plate was evaluated by the calculation of MIC. The control agar plates are necessary and were prepared similarly to the disc diffusion assay; however, the active ingredients had to be added to the well at different volumes.

In this study, the determination of antimicrobial activity of the bark extract serves as the intermediate control in the evaluation of antimicrobial activity of the synthesized AgNPs. Consequently, the positive and negative controls were maintained as described above for the experiments.

#### 2.3.3. Synthesis of AgNPs

The first step in the synthesis of AgNPs is the preparation of a 1 mM silver nitrate ( $\text{AgNO}_3$ ) solution. To prepare 1 mM of the  $\text{AgNO}_3$  solution, 0.0085 g of  $\text{AgNO}_3$  powder was dissolved in 25 mL of distilled water. For the preparation of *S. trilobatum* extract-capped AgNPs, 0.5 mL of the bark extract was added along with 2.5 mL of an  $\text{AgNO}_3$  solution into a Falcon tube. Then, 2 mL of distilled water was added to the mixture. The Falcon tube was immediately covered with aluminum foil. The solution was homogenized gently and kept at room temperature. The reaction between *S. trilobatum* bark extract and silver metal ions from  $\text{AgNO}_3$  results in a color change of the solution from pale yellow to brown. The color change could indicate the formation of AgNPs in the solution. It was necessary to maintain a control where no bark extract solution was added to the  $\text{AgNO}_3$  solution, which would show no color changes. Next, the reaction mixture was centrifuged at 10000xg for 10 min using a microcentrifuge. After centrifugation, the supernatant was discarded, and the pellet of AgNPs was washed thoroughly. The tubes were centrifuged again at 10000 rpm for 10 min, and the supernatant was discarded. This step was repeated three times to remove the impurities and collect the purified AgNP pellet. After the final washing and centrifugation, the pellets were air dried and stored at 4 °C for further experimentation.

### 2.4. Characterization of AgNPs

TEM was used to examine the nanoparticle's surface morphology and measure the size of AgNPs. TEM analysis was performed on a JEM-2100F, JEOL, Japan. TEM and Selected Area Electron Diffraction (SAED) images were taken during operation at a voltage of 200 kV. A transmission electron microscope equipped with X-ray energy dispersive spectrometer (EDX) was used to evaluate the elemental composition of AgNPs. The EDX analysis was performed using EDS, Oxford Inca Energy, England.

FESEM was used to confirm the shape and configuration of AgNP synthesized. A field emission scanning electron microscope (Hitachi, S-4300 SE, Japan) scans AgNPs with high-energy electron beams via a beam focused on the sample. FESEM images of AgNP were taken under a high-energy electron beam at 15 kV and a working distance of 6.6 mm. The samples were prepared on an aluminum grid and dried before the microscopic observation. The elemental composition of the nanoparticles was analyzed using EDX (EDAX, USA).

The AgNPs synthesized using the bark extract solution were examined by AFM (NanoScope, Ica, Veeco, USA). A thin pellet of AgNPs was prepared on a glass slide, and was allowed to dry for 5 min; the slides were then scanned by AFM to analyze the 3D structure of AgNPs.

The crystalline nature of the eco-friendly synthesized AgNPs

was analyzed by means of XRD patterns, and for these measurements, we used an XRD DMAX-2500, Rigaku, Japan, equipped with a nickel filter and Cu K $\alpha$  ( $\lambda = 1.54056 \text{ \AA}$ ) radiation source. The diffraction angle was varied in the range of 10–60° at 40 kV and 100 mA.

The development of AgNPs in the reaction mixture was identified by means of a UV–visible spectrophotometer (UV–Vis Lambda 35, Perkin Elmer, USA). The sampling of the reaction mixture by UV–visible spectroscopy was carried out to analyze the bio-reduction of the aqueous silver ion to metallic AgNPs. The highest peak of absorption in the UV spectrum should show the highest AgNP concentration in the reaction mixture (the highest yield). To study the visible region of *S. trilobatum* extract-capped AgNPs in the electromagnetic spectrum, the wavelength range of the UV–visible spectrophotometer was scanned from 200 to 900 nm to obtain the highest absorbance intensity of AgNP.

FTIR was used in order to examine the molecular configuration of AgNPs. FTIR (Spectrum 65, Perkin Elmer, USA) records the infrared spectrum of AgNPs by either absorption or emission of a sample. It is necessary to make a KBr pellet with AgNPs to study the FTIR spectrum from 4000 to 650  $\text{cm}^{-1}$ .

*S. trilobatum* extract-capped AgNPs were analyzed by XPS (Thermo Scientific, K-Alpha, UK) was equipped with Aluminium X-ray source operated at 72 W, to identify the elemental and chemical bonding on the surface of the AgNPs synthesized. The AgNP samples for XPS were prepared on a silicon (Si) wafer dropwise, followed by drying of the AgNP suspension.

The size distribution and stability of AgNPs were determined by dynamic light scattering (DLS) using Zeta potential and particle size analyzer, Photal Otsuka Electronics, ELC-Z model, Japan. The freeze-dried pellet of AgNP was dispersed with water to attain a proper scattering intensity before the measurement.

## 2.5. Antimicrobial activity of *S. trilobatum* extract-capped AgNPs

### 2.5.1. Serial dilution of AgNPs

To study the antimicrobial activity of *S. trilobatum* extract-capped AgNPs, a serial dilution was carried out for the AgNPs synthesized. Five Eppendorf tubes were labeled 2, 3, 4, and 5. Next, 500  $\mu\text{L}$  of sterile distilled water was pipetted into an Eppendorf tube containing the pellet of AgNPs and the pellet was resuspended. This tube was labeled as tube 1. Then, 250  $\mu\text{L}$  of the solution from tube 1 was pipetted into tube 2 and at the same time, 250  $\mu\text{L}$  of sterile distilled water was also pipetted into tube 2. These steps were repeated for the other dilutions. The solution from each tube was used for the determination of antimicrobial activity.

### 2.5.2. Determination of antimicrobial activity of AgNPs

The disc diffusion and well diffusion assays for *E. coli* and *Bacillus* sp. were performed according to the procedure described above using the bark extract-capped AgNPs. The antimicrobial activity of AgNPs was studied in comparison with the antimicrobial activity of the bark extract by analyzing the zone of inhibition formed in the agar plates. As mentioned earlier, it was necessary to incubate a control plate with ampicillin as the positive control for the experiment. The experiments were carried out in triplicate to obtain statistics.

### 2.5.3. Synthesis of AgNPs by the chemical method

The chemical synthesis of AgNPs was performed during the experimentation to compare the properties and characteristics of AgNPs after the green synthesis. Preparation of AgNPs by the chemical method involves reduction of silver ions to metallic AgNPs by a strong reducing agent. In this experiment, sodium borohydride ( $\text{NaBH}_4$ ) was used as a reducing agent. A 1 mM silver

nitrate ( $\text{AgNO}_3$ ) solution was prepared by dissolving 0.0085 g of  $\text{AgNO}_3$  powder in 50 mL of distilled water. Next, 0.002 M  $\text{NaBH}_4$  was prepared by dissolving 0.0023 g of  $\text{NaBH}_4$  powder in 30 mL of distilled water in an Erlenmeyer flask. Magnetic stirrer bar was placed into the Erlenmeyer flask, and the flask was placed in an ice bath on a stirring plate. The ice bath was used to slow down the reaction and gain better control over the final particle size/shape. The liquid was incubated by stirring for 20 min, which eventually cooled the liquid. Then, 2 mL of the 1 mM  $\text{AgNO}_3$  solution was added to the stirred  $\text{NaBH}_4$  solution at approximately 1 drop per second. The stirring was stopped as soon as all the  $\text{AgNO}_3$  was added. The reaction between  $\text{AgNO}_3$  and  $\text{NaBH}_4$  resulted in the reduction of silver ions in the solution and aggregation of metallic silver as monodisperse AgNPs. A few drops of a 1.5 M sodium chloride ( $\text{NaCl}$ ) solution were added to the test tube. The  $\text{NaCl}$  solution caused the suspension to turn dark yellow, then grey as the AgNPs aggregate. Then, a drop of 0.3% polyvinylpyrrolidone (PVP) solution was added to the suspension to prevent the aggregation. The suspension was transferred into a small beaker and kept in an oven at 50 °C overnight to obtain the pellet of AgNPs.

The AgNPs synthesized by the chemical method were analyzed for their structural and morphological characteristics using UV–visible spectroscopy, SEM, and FTIR. The results obtained from the characterization of AgNPs synthesized by the green method and chemical methods were analyzed to study the effect of *S. trilobatum* bark extract on the performance of the AgNPs synthesized. Beside the characterization, antimicrobial activity of AgNPs synthesized by the chemical method was also evaluated by conducting the disc diffusion assay on an *E. coli* agar plate. The results were compared with the antimicrobial activity of *S. trilobatum* extract-capped AgNPs.

## 3. Results and discussion

### 3.1. Antimicrobial activity of *Solanum trilobatum* bark extract

The anti-infection properties of the bark extract prepared here were evaluated using pathogenic bacteria and fungi. *E. coli* (opportunistic pathogen), *Bacillus* sp. (pathogen), and *A. niger* (pathogen) were used as the test microorganisms to determine the antimicrobial activity. The bark extract from the *S. trilobatum* herb showed inhibition of growth of all the tested microorganisms. The MIC of bark extract was found to be 5  $\mu\text{g}$  per 50  $\mu\text{L}$ . The extent of antimicrobial activity of the bark extract solution was determined by measuring the zone of inhibition in millimeters (mm). In terms of antibacterial activities, the bark extract inhibited the growth of both *E. coli* and *Bacillus* sp. and the results were tabulated in Table 1. In the disc diffusion assay, the zone of inhibition of *E. coli* was larger than in *Bacillus* sp. by 1.25 mm with bark extract concentration 5  $\mu\text{g}$  per 50  $\mu\text{L}$ . The variation among the zone of inhibition between *E. coli* and *Bacillus* sp. can be explained by the cell wall nature of these bacteria. *E. coli* is a gram-negative bacterium and the structure of its cell wall consists of a thin layer of peptidoglycans between the inner and outer layer of lipid membranes. *Bacillus* is a gram-positive bacterium, and its cell wall consists of a thick layer of peptidoglycan in the periplasmic space of the cell membrane. Due to the thin layer of peptidoglycan, the components of the bark extract can easily diffuse through the cell wall of gram-negative bacteria and impede the cellular function of the bacteria. The difference in the thickness of cell wall of gram positive and gram negative bacteria causes the zone of microbial inhibition for *E. coli* to be larger than that for *Bacillus* sp. The bark extract solution inhibited both bacteria only in the disc diffusion assay. It seems that the bark extract solution was not strong enough to diffuse through the agar wells to inhibit the bacteria. Thus, no obvious inhibition

**Table 1**  
Measurements of the zone of inhibition caused by the bark extract, AgNPs, and ampicillin.

Zone of inhibition (mm), bark extract				
Concentration ( $\mu\text{g}$ )	<i>E. coli</i>		<i>Bacillus</i> sp.	
	Well diffusion	Disc diffusion	Well diffusion	Disc diffusion
5	0	9.0 ( $\pm 1.5$ )	10.0 ( $\pm 1.0$ )	7.5 ( $\pm 1.2$ )
2.5	0	6.5 ( $\pm 1.0$ )	8.0 ( $\pm 0.5$ )	7.0 ( $\pm 1.0$ )
1.25	0	0	0	6.2 ( $\pm 0.5$ )
0.63	0	0	0	0.6 ( $\pm 0.3$ )
0.31	0	0	0	0
H <sub>2</sub> O	0	0	0	0
Zone of inhibition (mm), ampicillin				
Concentration ( $\mu\text{g}$ )	<i>E. coli</i>		<i>Bacillus</i> sp.	
	Well diffusion	Disc diffusion	Well diffusion	Disc diffusion
100	18.0 ( $\pm 5.0$ )	14.5 ( $\pm 4.5$ )	9.75 ( $\pm 1.0$ )	9.0 ( $\pm 1.25$ )
80	17.0 ( $\pm 4.75$ )	9.5 ( $\pm 2.5$ )	0	6.5 ( $\pm 0.5$ )
60	16.5 ( $\pm 4.0$ )	9.25 ( $\pm 2.0$ )	0	8.0 ( $\pm 1.0$ )
40	15.1 ( $\pm 4.0$ )	8.0 ( $\pm 1.5$ )	0	7.75 ( $\pm 0.75$ )
20	13.0 ( $\pm 2.5$ )	7.0 ( $\pm 1.0$ )	0	6.25 ( $\pm 0.25$ )
2	0	10.0 ( $\pm 2.5$ )	0	0
H <sub>2</sub> O	0	0	0	0
Zone of inhibition (mm), AgNPs				
Concentration <sup>a</sup> ( $\mu\text{g}$ )	<i>E. coli</i>		<i>Bacillus</i> sp.	
	Well diffusion	Disc diffusion	Well diffusion	Disc diffusion
5	13.0 ( $\pm 2.0$ )	11.75 ( $\pm 4.0$ )	12.5 ( $\pm 2.0$ )	12.0 ( $\pm 3.25$ )
2.5	11.75 ( $\pm 1.25$ )	11.0 ( $\pm 3.0$ )	11.0 ( $\pm 1.75$ )	8.0 ( $\pm 1.0$ )
1.25	11.0 ( $\pm 1.0$ )	0	10.0 ( $\pm 1.0$ )	0
0.63	11.0 ( $\pm 1.0$ )	0	8.0 ( $\pm 0.25$ )	0
0.31	9.0 ( $\pm 0.75$ )	0	0	0

Values in the parentheses were calculated from triplicate experiments.

<sup>a</sup> The concentrations of AgNPs were calculated based on the bark extract used.

was observed in the well diffusion assay in the antimicrobial assay of the bark extract. Fig. 1a&b, shows the growth inhibition by the bark extract solution for both bacteria and the difference in the peptidoglycan layer. On the other hand, the antifungal properties of the bark extract solution were determined using *A. niger* (Fig. 2a). The bark extract only showed the antifungal activity in the well

diffusion assay and was unable to inhibit the growth of fungi in the disc diffusion assay. Literature has proven that the disc diffusion assay is unable to determine antifungal properties for all species of fungi [8]. It supports the current results of not able to determining the antifungal properties of the bark extract solution against *A. niger*. The antimicrobial activity of the *S. trilobatum* bark extract

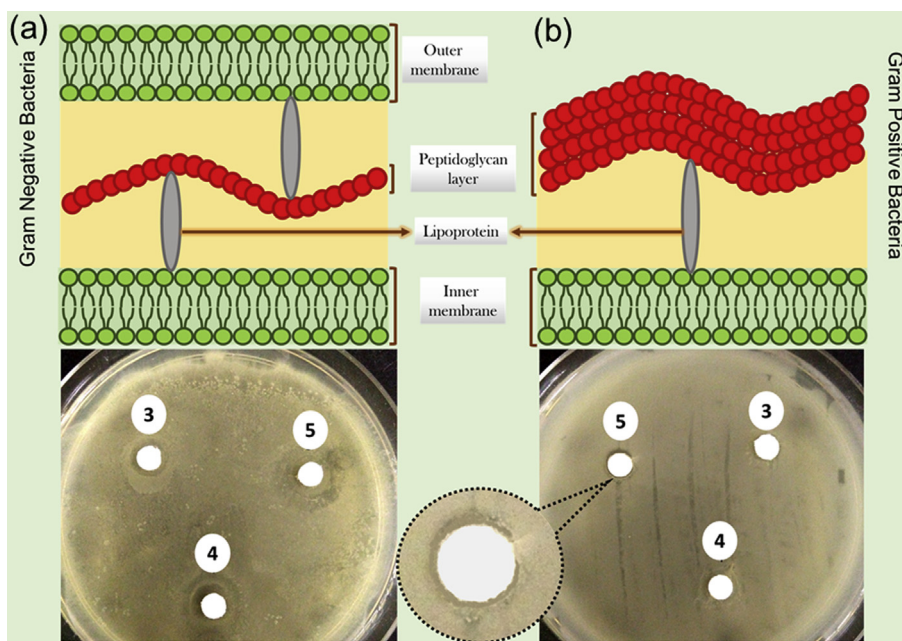


**Fig. 1.** Antimicrobial activity of bark extracts. (a) *Escherichia coli*; (b) *Bacillus* sp. The difference in the cell wall of gram-positive and gram-negative bacteria is shown. Numbers on the plates mean 1.25, 2.5, and 5  $\mu\text{g}$  per disc, respectively, for 3, 4 and 5. The inset shows an enlarged inhibition zone.

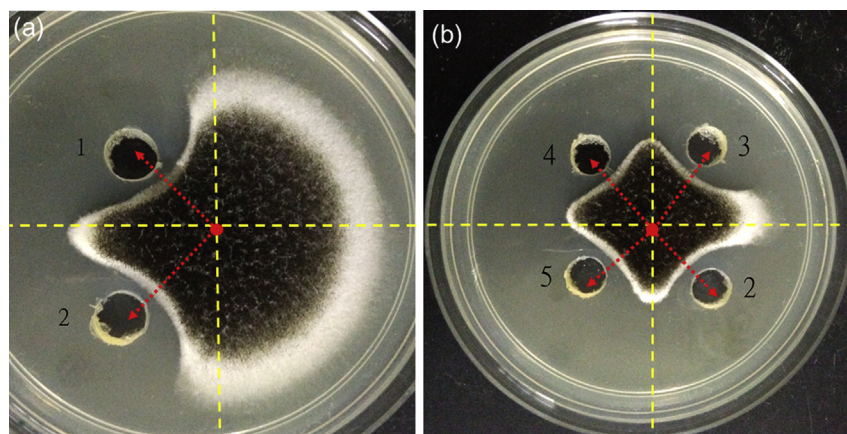


**Fig. 2.** Antifungal activity against *Aspergillus niger* on a PDA agar plate. (a) The bark extract. Numbers on the plates denote 0.63 and 0.31  $\mu\text{g}$  per disc, respectively for 1 and 2. (b) Ampicillin. Numbers on the plates indicate 40, 60, 80, and 100  $\mu\text{g}$  per disc, respectively, for 2, 3, 4 and 5. Red arrows indicate the measured regions from the inoculum point and the center of the well. (For interpretation of the references to color in this figure legend, the reader is referred to the Web version of this article.)

solution was compared with a positive control, ampicillin. Ampicillin has shown significant antimicrobial activity against *E. coli* but a lower microbial inhibition of *Bacillus* sp. growth in both disc and well diffusion assays (Fig. 3a&b). Figs. S1 and S2 show the antimicrobial activity of ampicillin against *E. coli* and *Bacillus* sp. in the disc and well diffusion assay, respectively. The zones of inhibition observed were clearer and larger as compared to the microbial inhibition caused by the bark extract solution in the disc diffusion assay. Fig. 2a&b shows that the bark extract solution and ampicillin clearly inhibited the growth of *A. niger* on the PDA agar plate in the well diffusion assay. The microbial inhibition by the bark extract solution at 5  $\mu\text{g}$  per 50  $\mu\text{L}$  was the same as the zone of inhibition of ampicillin at 0.125  $\mu\text{g}/\mu\text{L}$ , where the measured zone of inhibition was 7.5 mm. This result implies that the strength of bark extract was similar to that of ampicillin at 0.125  $\mu\text{g}/\mu\text{L}$ .

### 3.2. Visual identification of the synthesis of AgNPs

The assays of AgNPs are based on the color change of the reaction mixture. The suitability of the herb extract for the synthesis of AgNPs was confirmed by the changes in the color of the reaction mixture (silver nitrate ( $\text{AgNO}_3$ ) solution and bark extract) from colorless to brown. There was no immediate color change once the

bark extract solution was added to the  $\text{AgNO}_3$  solution. However, the solution started to turn slightly brown 30 min after the addition of the bark extract solution. As the intensity of brown color increased after 30 min, the bark extract solution caused chemical reduction of silver ions to AgNPs in the solution. After 24 h, the color of the solution turned dark brown and a layer of synthesized AgNP was seen settling down at the bottom of the falcon tube (Fig. 3; inset). After microcentrifugation of the reaction mixture, the pellet of AgNPs was collected at the bottom of an Eppendorf tube.

### 3.3. Characterization of AgNPs

#### 3.3.1. TEM

The size and shape of *S. trilobatum* extract-capped AgNPs were studied using the TEM. Fig. 4 (a–c) shows the image of biologically synthesized AgNPs, where the lattice fringes of a nanoparticle are shown precisely. The TEM image reveals that the AgNPs synthesized were spherically shaped particles with smooth edges. The images at different magnification of TEM showed that almost all the AgNPs synthesized had a nearly spherical shape and similar ranges of sizes. TEM images suggested that the synthesized AgNPs were well dispersed without aggregates of the nanoparticles. The sizes of the AgNPs ranged between ~10 and ~50 nm with an average size of

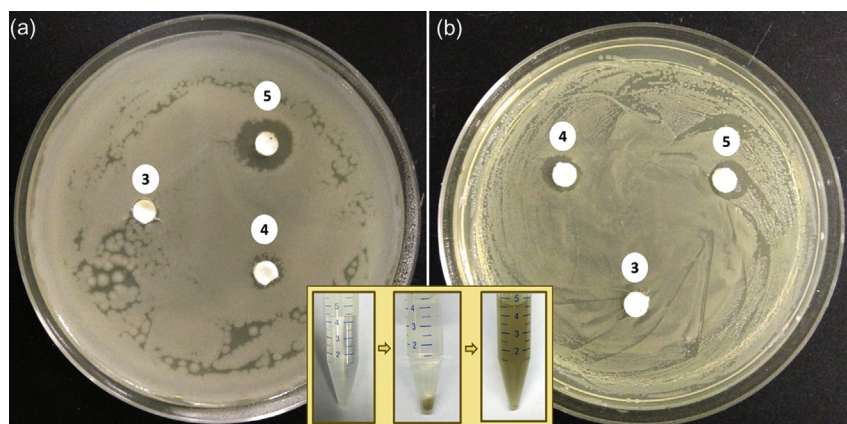


**Fig. 3.** Formation of AgNPs and their antibacterial activity. Antimicrobial activity of eco-friendly synthesized AgNPs against (a) *E. coli* and (b) *Bacillus* sp. Numbers on the plates denote 1.25, 2.5, and 5  $\mu\text{g}$  per disc, respectively, for 3, 4 and 5. The inset shows confirmation by the changes in the color of the reaction mixture, which turned dark brown and a layer of synthesized AgNPs was seen to settle down at the bottom of the Falcon tube. (For interpretation of the references to color in this figure legend, the reader is referred to the Web version of this article.)

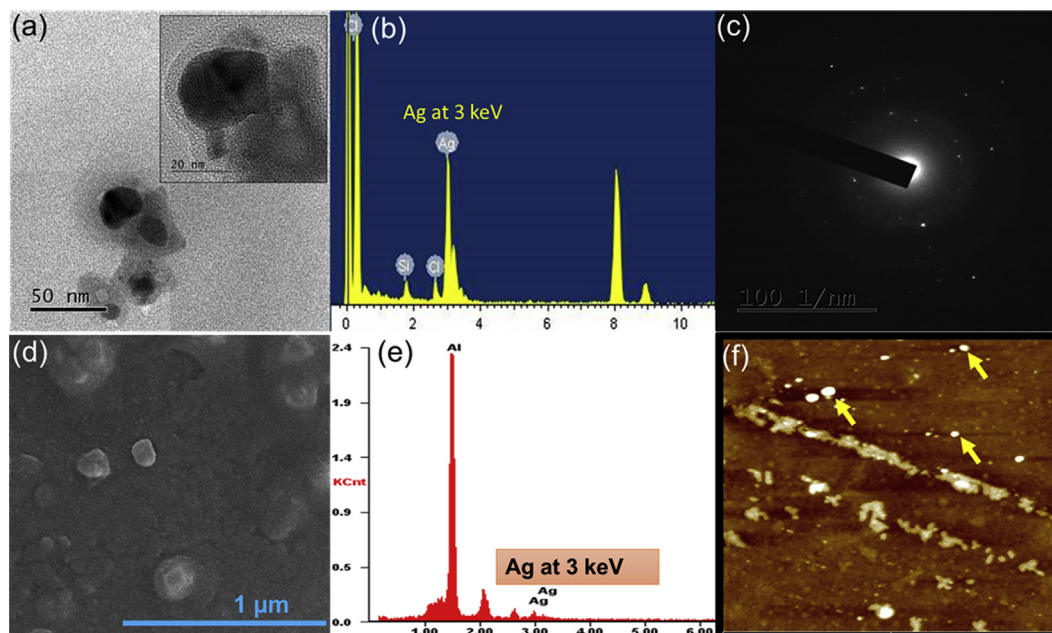


**Fig. 4.** Morphological features of eco-friendly synthesized AgNP. (a) A TEM image at the 50- and 20-nm scale (inset); (b) EDX analysis by TEM; (c) SAED analysis of AgNPs by TEM; (d) A FESEM image of AgNPs at 1- $\mu$ m scale; (e) EDX analysis by FESEM; (f) spherical AgNPs observed by means of AFM (indicated with arrows).

~25 nm. There were a few traces of AgNP clusters in the image, which are expected to influence the variation in particle size of AgNPs. The calculation of the size of AgNP was done in accordance with the size observed in the TEM images. Fig. 4c shows a selected area electron diffraction (SAED) pattern of the synthesized particles. The individual bright spots in the image clearly indicate that the AgNPs are crystalline in nature. Fig. 4b shows the EDX analysis (after TEM) of biologically synthesized AgNPs using the *S. trilobatum* bark extract. EDX analysis revealed the quantitative status of the elements that may be involved in the formation of AgNPs. It is used to determine the amount of each element present in an AgNP. The peak intensity is proportional to the amount of AgNPs synthesized. The load of AgNPs formed is dependent on the amount of silver present in the solution. The EDX spectra confirmed the formation of AgNPs. The peak raised at 3 keV is due to silver and confirms the formation of bioreduced AgNPs. Generally, metallic silver nanocrystals have a typical optical absorption peak at ~3 keV due to SPR.

### 3.3.2. FESEM

FESEM analysis was also applied to evaluate the shape of the nanoparticles synthesized. Fig. 4 (d&e) shows a high-density image of AgNPs synthesized using the *S. trilobatum* bark extract solution. The images clearly depict the relatively spherical and uniform shape of the synthesized AgNPs. Based on FESEM images, the size of the synthesized AgNPs was between 50 and 100 nm in diameter: it is larger than the size determined by TEM. The larger size of AgNPs may be due to the aggregation of AgNPs and the measurement of clustered AgNPs by FESEM. Fig. 4e shows a FESEM elemental profile of AgNPs biologically synthesized by means of the *S. trilobatum* bark extract solution. The spectral line at 3 keV is increased due to AgNPs. The spectral line of Al observed at 1.5 keV may arise due to the sample grid holder which is made from an Al alloy.

### 3.3.3. AFM

AFM was used for specific examination of surface roughness and morphology of biologically synthesized AgNPs. The size of AgNPs based on AFM analysis was ~25 nm in diameter. This means that the

size of AgNPs is close to the size of particles estimated by means of FESEM and TEM images. The resolution of AFM revealed clustered AgNPs where the individual AgNPs appears as a small spot of spherical shape. Unlike SEM and TEM, AFM provides an accurate and precise measurement of the height of a nanoparticle. Based on Fig. 4f, the height of synthesized AgNPs is ~20 nm for a sharp and rough end of the particle.

### 3.3.4. XRD

Fig. 5 shows XRD patterns of *S. trilobatum* extract-capped AgNPs. Five main diffraction peaks for Ag were observed at  $2\theta = 27.81, 32.19, 46.17, 51.59,$  and  $56.11$ , which correspond to the planes of face-centered cubic (fcc) Ag crystals at  $75.06, 103.35, 55.64, 46.14,$  and  $39.93$ , respectively. In general, the diffraction peaks of XRD patterns are related to crystallite size of AgNPs. The Debye-Scherrer equation was used to determine average crystallite diameter from the half width of the diffraction peaks. The Debye-Scherrer equation is

$$D = \frac{k\lambda}{\beta \cos\theta}$$

where D stands for the crystallite size of the powder,  $\lambda$  is the wavelength of  $\text{CuK}\alpha$ ,  $\beta$  is the full width at half-maximum (FWHM),  $\theta$  is the Bragg diffraction angle, and k is a constant. The wavelength of  $\text{CuK}\alpha$  is constant where  $\lambda = 1.5412 \text{ \AA}$ ; k is the Scherrer constant, which depends on how the width is determined, the shape of the crystal, and the size distribution. The common value of k is 0.9 for FWHM of spherical crystals with cubic symmetry. The equation was used to calculate the average crystallite size of AgNPs. The diffraction peaks of XRD can be used to calculate the interplanar spacing between the atoms (d-spacing) using Bragg's law. The equation for calculating d-spacing is

$$2d \sin \theta = n\lambda \quad (n = 1)$$

where  $\lambda$  is the wavelength of  $\text{CuK}\alpha$ . The table (inset of Fig. 5) shows the calculated values of d-spacing and crystallite size for the

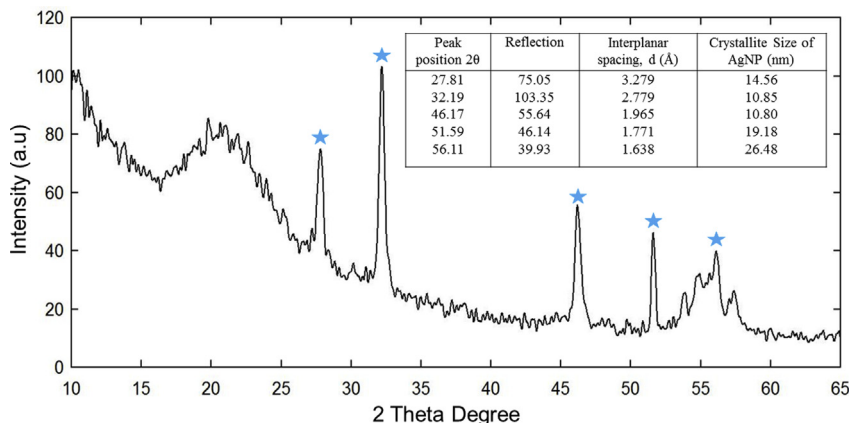


Fig. 5. An XRD pattern of eco-friendly synthesized AgNPs. The table inset shows the calculated interplanar spacing and crystallite size of AgNPs. Peaks are indicated with asterisks.

synthesized AgNPs. Based on the calculated values, the average crystallite size for AgNPs was found to be within 20 nm.

### 3.3.5. UV–visible spectroscopy

UV–Visible spectroscopy is one of the elementary approaches to analyze synthesized AgNPs. The synthesis of AgNPs was confirmed by the positioning of the surface plasmon resonance (SPR) in the UV–Vis spectroscopic analysis (Fig. 6a–c). The synthesis of *S. trilobatum* bark extract-capped AgNPs was evidenced as a peak observed at 442 nm (Fig. 6a). The peak in the UV spectrum increased due to the effects of surface plasmon resonance of electrons in the AgNP solution. The peak formed in the UV–Visible spectrum is influenced by the size, shape, and morphology of the AgNPs being synthesized. Some studies have proven that the visible region of AgNP absorbance in UV–Visible spectroscopy is 400–450 nm. The broad range of the absorption band corresponds to various sizes and shapes of AgNPs [9]. The spherical shaped AgNPs contributes to the absorption band at around 400–420 nm in the UV–Visible spectrum [10]. The absorption band for the reaction mixture of the brown solution should be at ~485 nm if there are any impurities in the mixture [11]. The centrifugation and washing of AgNPs removed the impurities in the form of the supernatant. The pellet, when re-dispersed in water, showed well-defined SPR at 442 nm. The bark extract was also analyzed by UV–Visible spectroscopy. Fig. 6c indicates that the peak at 240 nm was observed in both AgNPs and in the bark extract solution. The peak at 240 nm in both spectra indicates the presence of amino acid residues as herbal extract components [12]. The amino acids in the

bark extract solution are expected to serve as the reducing and stabilizing agent for the AgNP synthesis. The visible region of the absorption of the AgNP synthesized by the chemical method was also analyzed by UV–Visible spectroscopy. The peak was observed at 405 nm in the spectrum shown in Fig. 6b. The visible region of absorption of AgNPs synthesized by both biological and chemical methods falls within the range of 400–450 nm. Therefore, it is expected that the morphological characteristics of both types of synthesized AgNPs were similar. The results of the biological method were then validated by microscopic analyses.

### 3.3.6. FTIR

FTIR spectra provide sufficient information on the biomolecules present in AgNPs. In this work, the spectra generated by FTIR were analyzed to identify the organic compounds present on the nanoparticles, which may be responsible for the reduction of silver ions to metal and for capping the bioreduced AgNPs. In Fig. 7, the FTIR spectra generated for AgNPs and for the bark extract are presented. The FTIR spectra for AgNPs showed prominent peaks at 1225 and 1363  $\text{cm}^{-1}$  (marked with a pentagon). The absence of a visible peak at 1225 and 1363  $\text{cm}^{-1}$  in the IR spectra of the bark extract solution means that the peak visible in the AgNP spectrum resulted from the addition of silver nitrate ( $\text{AgNO}_3$ ) solution during the synthesis of AgNPs; therefore, it proves the presence of silver on AgNPs. On the contrary, the FTIR spectra of the bark extract solution contained distinct peaks at 1050 and 688  $\text{cm}^{-1}$  (marked with triangles). Similar peaks at 1050 and 688  $\text{cm}^{-1}$  also appeared in the FTIR spectra of bioreduced AgNPs. The observation of complementary

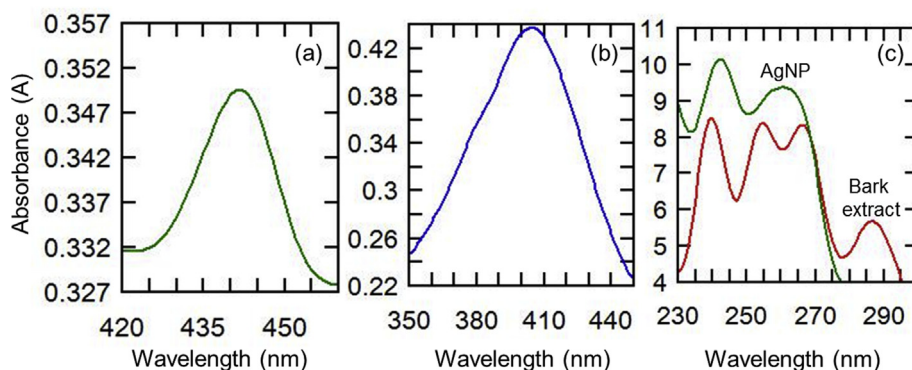
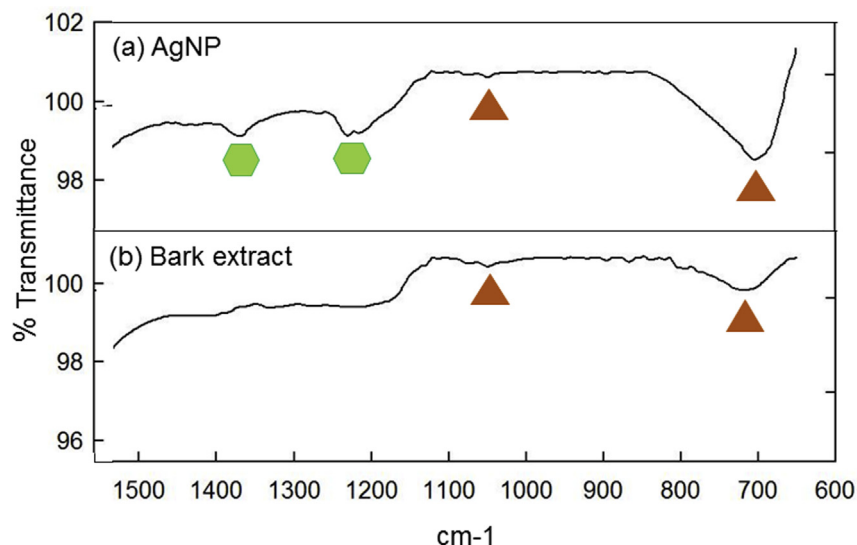


Fig. 6. UV–Visible spectra of (a) eco-friendly synthesized AgNPs; (b) chemically synthesized AgNPs, and (c) the SPR peak observed for both AgNPs and the bark extract solution. Scanned in the respective ranges.



**Fig. 7.** FTIR spectra of (a) green synthesized AgNP and (b) *S. trilobatum* bark extract. Green octagonal represents different peak positions. (For interpretation of the references to color in this figure legend, the reader is referred to the Web version of this article.)

peaks in the two spectra shows that the biomolecules present in the bark extract solution are also present in AgNP. The identical peaks confirmed that the bark extract components act as a bio-based reducing agent for green synthesis of AgNPs and stabilize the AgNPs synthesized to prevent aggregation.

### 3.3.7. XPS

*S. trilobatum* extract-capped AgNPs were analyzed by XPS (Thermo Scientific, K-Alpha, UK) to identify the changes in surface composition. Fig. 8a indicates that oxygen, silicon, and carbon have prominent peaks whereas silver and nitrogen show weaker signals from the surface of the AgNPs in the survey scan. Fig. 8b shows that the binding energies of Ag 3d<sub>3/2</sub> and Ag 3d<sub>5/2</sub> were 367.7 and

373.7 eV, respectively. The formation of metallic silver on the surface of the synthesized AgNPs is confirmed since slitting of the 3d doublet of Ag was 6.0 eV ( $\Delta$  metal = 6.0 eV). Based on Fig. 8c, the peak for O1s was observed at 532.9 eV. The peak indicates the presence of carbonyl groups on the surface of AgNPs. Besides 532.9 eV, there was no peak observed in the O1s scan, which corresponds to the absence of metallic oxides or carbonates on the surface of AgNPs. The presence of silver on the AgNP surface was less prominent, perhaps due to the ability of oxygen to oxidize silver. The tremendous ability of oxygen to oxidize silver may reduce the proportion of silver on the surface of an AgNP [13]. Nevertheless, the analysis of EDX by FESEM and TEM showed the dominating silver component on the AgNP synthesized. Fig. 8d

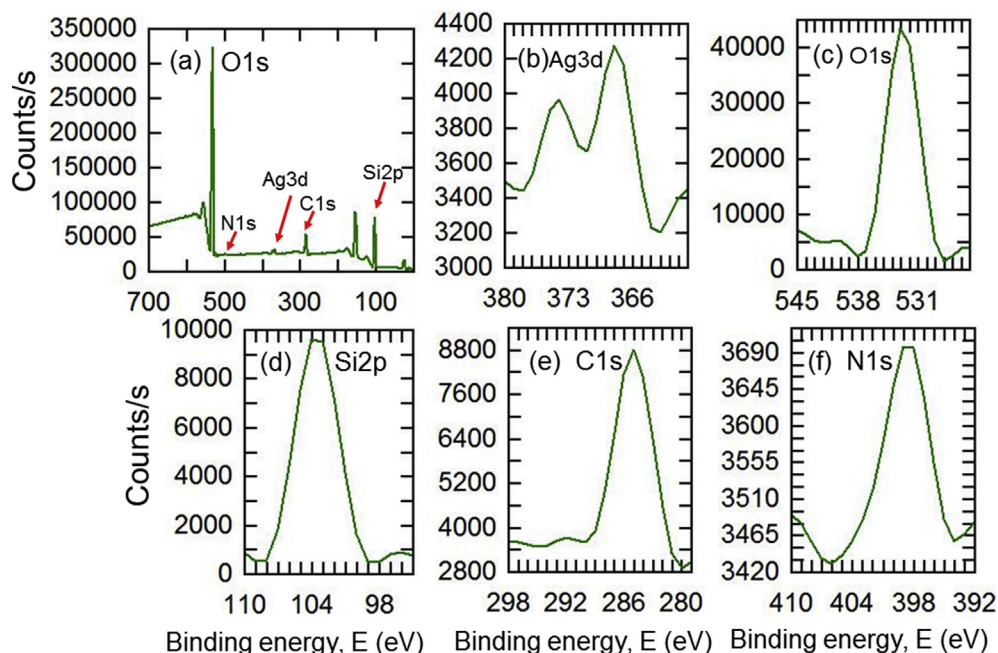


**Fig. 8.** XPS data for eco-friendly synthesized AgNPs. (a) A survey scan, (b) silver Ag3d data, (c) oxygen O1s data, (d) silicon Si2p data, (e) carbon C1s data, and (f) nitrogen N1s data. (For interpretation of the references to color in this figure legend, the reader is referred to the Web version of this article.)

shows the asymmetric peak of Si2p at 103.65 eV which corresponds to the existence of silicon oxide on the surface of AgNP. The next apparent spectrum is the C1s scan. Fig. 8e represents the peak for the C1s scan observed at 284.9 eV. AgNPs that have been exposed to the atmosphere will have a detectable quantity of adventitious carbon contamination typically with a layer thickness of 1–2 nm. The peak at 284.9 eV corresponds to the C–C components, by default. Nevertheless, it is possible to have C–O–C and O–C=O components on carbon-contaminated AgNPs. The final and least abundant element revealed by XPS spectra is nitrogen as shown in Fig. 7f. The wide width and intensity range of the N1s peaks on the surface of AgNPs may be attributed to N–C and N–S bonds [14–16].

### 3.3.8. Zeta potential measurements

The particle size of AgNP synthesized was diagnosed by DLS. When AgNP dispersed in water, it exhibits a Brownian motion, which can be measured by the fluctuations in the intensity of the scattered light. Eventually, the particle size is calculated by Stokes-Einstein equation which correlates with the translational diffusion coefficient [17]. Based on Fig. 9, the size of AgNP synthesized is 285.4 nm in diameter. Particle size distribution showed the presence of AgNP with polydispersity index (PDI) value of 0.154. The PDI value indicates the range nanoparticle size distribution. A higher value of PDI reflects a wider range of particles whereas a lower value of PDI reflects samples with evenly sized particles. The lower of PDI obtained for AgNP synthesized indicates that monodispersed AgNPs have greater particle stability [18]. Moreover, the stability of nanoparticle is well explained by the measurement of the magnitude of electrostatic charge attraction or repulsion between the particles in the liquid medium. The measurement is expressed as zeta potential. Particles with zeta potentials higher than +30 mV and lower than –30 mV are the indicative of stable AgNPs. The zeta potential obtained for green synthesized AgNP in this study was –16 mV indicating that the AgNPs were stable, which is proven by narrow size distribution index.

### 3.4. Antimicrobial activity of *Solanum trilobatum* extract-capped silver nanoparticle

The antimicrobial activities of AgNPs synthesized using the bark extract as a reducing agent was analyzed too. The AgNPs were synthesized using 5 µg per 50 µL concentration since this is the

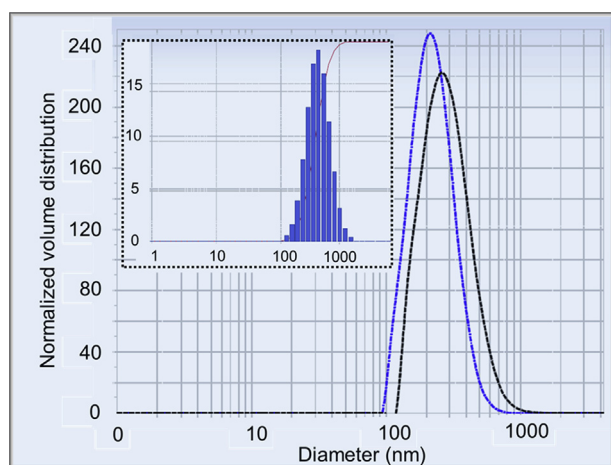


**Fig. 9.** Mean particle size of the green synthesized AgNP under DSL studies. Figure inset is the intensity distribution of diameter for AgNP. (For interpretation of the references to color in this figure legend, the reader is referred to the Web version of this article.)

confirmed MIC for the herbal extract. The *S. trilobatum*-capped AgNPs showed significant antimicrobial activity against the tested microorganisms. The zones of inhibition were observed apparently for both gram-positive and gram-negative bacteria. The results on the antimicrobial activity of AgNP against *E. coli* and *Bacillus* sp. were interpreted by measuring the zone of inhibition in millimeters (mm). Our synthesized AgNPs were capable of inhibiting the bacterial growth according to both disc diffusion and well diffusion assays. The results on the zone of inhibition for both assays using *E. coli* and *Bacillus* sp. are tabulated in Table 1. The highest concentration of AgNP showed the most significant zone of inhibition toward *E. coli* and *Bacillus* sp. Fig. 3 shows inhibition of the microbial growth by AgNP toward *E. coli* and *Bacillus* sp. in a disc diffusion assay and the formation of AgNP with color changes in the reaction mixture. Nonetheless, there were differences in the zone of inhibition between *E. coli* and *Bacillus* sp. agar plates in disc and well diffusion assays. As stated above, the thick peptidoglycan layer in the gram-positive bacteria cell wall causes difficulties for AgNPs during diffusion through the cell wall, disrupts the function of the bacterial cell, and inhibits its growth. Therefore, the zone of inhibition for *E. coli* was larger than that for *Bacillus* sp. in both disc and well diffusion assays. Fig. S3 shows the microbial growth inhibition by AgNP in a well-diffusion assay. Nonetheless, the highest concentration of AgNPs has yielded almost equal measured size of the zone of bacterial inhibition. Based on the measured zone of inhibition, it can be concluded that the 0.1 µg/µL AgNPs cause microbial growth inhibition that is similar to that of ampicillin at 0.25 to 0.125 µg/µL in both disc and well diffusion assays against *E. coli* and *Bacillus* sp.

The comparison of antimicrobial activities of the bark extract and of the eco-friendly synthesized AgNPs was carried out. The zone of inhibition yielded by AgNPs was larger than that of the bark extract. As stated above, the bark extract is a natural anti-infection ingredient where the extent of microbial inhibition is obviously lower than that of a purified anti-infection component. On the other hand, AgNPs showed a significant inhibition zone as compared to the bark extract solution. The properties of AgNPs can explain the antimicrobial activity of AgNPs. For instance, AgNPs have stronger penetrating properties and a larger surface area per volume. It enables the AgNPs to easily diffuse through the cell wall of microorganisms and to disrupt the function of microbial cells. Because the plant extract solution is a natural compound with multiple components and has a weaker penetration ability when compared to AgNPs, the plant extract components diffuse through the cell wall of bacteria via a complicated route and are unable to damage the bacterial cell.

The mechanism of AgNPs' antimicrobial activity is still ambiguous. However, it is widely accepted that AgNPs can attach to and subsequently penetrate into the bacterial cell wall through the periplasmic space of the cell wall into the cytoplasm thus causing the formation of "pits" in the structure of the cell membrane. This action increases the cell permeability for more AgNPs to diffuse into the cell and leads to malfunction of bacterial cells [19]. Another mechanism of AgNP-driven changes in the cell wall of bacteria is the formation of free radicals by AgNPs. These nanoparticles can release a free radical when they are in contact with the cell wall of a microorganism. The ability of free radicals to damage the cell wall of bacteria makes the cell surface more porous and permeable to external compounds and leads to cell death [20]. The mechanism of AgNP-mediated disruption of the cellular function of microorganisms is also explained by the acid and base concept. Silver has mild acidic properties by nature. AgNPs formed by reduction of silver ions also have acid properties when they are in contact with other components. On the other hand, DNA of cells consists of bases such as sulfur and phosphorus as their major components. Here, AgNPs

diffuse through the cell membrane and may act on the base components of DNA and thus terminate the DNA replication in the bacterial cell and thus results in the death of bacteria [21,22].

### 3.5. Green synthesis of AgNPs versus chemical synthesis

The antimicrobial activity of eco-friendly synthesized AgNPs was compared with that in the AgNPs synthesized by the chemical method. The disc diffusion assay on *E. coli* after chemical synthesis of AgNPs showed insignificant microbial inhibition. Fig. S4 indicates that there was no visible zone of inhibition for the chemically synthesized AgNPs against *E. coli*. The result proves that the antimicrobial activity of eco-friendly synthesized AgNPs is much stronger as compared to the antimicrobial properties of chemically synthesized AgNP. Green synthesis is also preferred as an effective method for production of AgNPs because of the presence of natural reducing and capping agents. They allow technologists to avoid the use of chemical reducing agents and stabilizing agents, which are used in the chemical synthesis of AgNPs. The presence of protein and starch components in the plant extract ensures superior antimicrobial properties for the synthesized AgNPs. Accordingly, green synthesis is known as an environmentally friendly synthesis method (in contrast to the chemical method) because of the bio-based reducing and stabilizing agents [23,24]. Green synthesis has a great potential for large-scale AgNP synthesis because it is a cost-effective method as compared to chemical synthesis, which requires the use of strong chemical agents [25,26]. In addition, different lines of novel study have been demonstrated with the AgNPs, such as hybrid nanocomposite [27], derivative of AgNP [28] shape and size controlled synthesis [23] and other downstream applications [29]. Further, the potential use of plant extracts can be applied with AgNP as shown for other nanomaterial [30–34].

## 4. Conclusions

The bark extracts of *S. trilobatum* were proved a promising reagent for the synthesis of well-defined AgNPs. Our results showed that the minimum concentration of 0.1 µg/µL of the bark extract is sufficient to inhibit microbial growth. The bark extract at the minimum inhibitory concentration was used as the biological reducing agent and hence the *S. trilobatum* extract-capped AgNPs were successfully synthesized. The green synthesis of AgNPs was developed via a cost-effective and environmentally friendly approach without the use of chemical reagents throughout the nanoparticle synthesis. UV–Visible spectroscopy analysis showed a peak at 442 nm, confirming the formation of AgNPs. TEM analysis revealed that the biosynthesized AgNPs are spherical and have an average size of ~25 nm in diameter. The shape of AgNP was then confirmed by FESEM and AFM analyses, whereby the XRD analysis confirmed the size of AgNPs. The elemental composition of the surface of the eco-friendly synthesized AgNPs was characterized by XPS analysis. The FTIR spectrum of both biosynthesized AgNPs and of the bark extract solution proved that the bark extract acts as a reducing and stabilizing agent for the green synthesis of AgNPs. Disc and well diffusion assays were carried out for evaluation of antimicrobial activities of AgNPs synthesized using biological and chemical methods. It was demonstrated that the zone of inhibition of the biosynthesized AgNPs is significantly larger than that of the bark extract and of AgNPs created by the chemical method. The results strongly confirmed that the green synthesis of *S. trilobatum* extract-capped AgNPs yields enhanced antimicrobial properties, i.e., inhibits the growth of pathogenic microorganisms. Hence, the use of medicinal and herbal plants for the synthesis of AgNPs may be a good rationale for their use in medical applications. The joint effects of both AgNPs and of the molecules from the plant extract

that are present on the surface of the eco-friendly synthesized AgNPs should be sufficient to combat a variety of pathogenic microorganisms.

## Acknowledgements

The author Periasamy Anbu would like to thank Inha University Research grant for language editing support.

## Appendix A. Supplementary data

Supplementary data related to this article can be found at <https://doi.org/10.1016/j.molstruc.2018.01.056>.

## References

- [1] A. Suominen, Y. Li, J. Youtie, P. Shapira, A bibliometric analysis of the development of next-generation active nanotechnologies, *J. Nanopart. Res.* 18 (2016) 270.
- [2] S. Gurunathan, J.W. Han, D.N. Kwon, J.H. Kim, Enhanced antibacterial and antibiofilm activities of silver nanoparticles against Gram-negative and Gram-positive bacteria, *Nanoscale Res. Lett.* 31 (2014) 373.
- [3] S. Ahmed, M. Ahmad, B.L. Swami, S. Ikram, A review on plants extract mediated synthesis of silver nanoparticles for antimicrobial applications: a green expertise, *J. Adv. Res.* 7 (2016) 17–28.
- [4] S. Ahmed, M. Ahmad, B.L. Swami, Green synthesis of silver nanoparticles using *Azadirachta indica* aqueous leaf extract, *J. Radiat. Res. Appl. Sci.* 9 (2015) 1–7.
- [5] P.S. Latha, K. Kannabiran, Antimicrobial activity and phytochemicals of *Solanum trilobatum* Linn, *Afr. J. Biotechnol.* 5 (2006) 2402–2404.
- [6] M. Ramar, B. Manikandan, P.N. Marimuthu, T. Raman, A. Mahalingam, P. Subramanian, S. Karthick, A. Munusamy, Synthesis of silver nanoparticles using *olanum trilobatum* fruits extract and its antibacterial, cytotoxic activity against human breast cancer cell line MCF 7, *Spectrochim. Acta* 140 (2015) 223–228.
- [7] G. Priya, C. Chellaram, Evaluation of antibacterial activity and phytochemical analysis of medicinal plant *Solanum trilobatum*, *Int. J. Pharm. Biotechnol.* 5 (2014) 354–359.
- [8] M. Pratheeba, K.U. Rani, B. Ramesh, Studies on antimicrobial and anticancer activity of *Solanum trilobatum*, *Asian J. Pharm. Clin. Res.* 7 (2014) 213–219.
- [9] M. Ramar, B. Manikandan, P.N. Marimuthu, T. Raman, A. Mahalingam, P. Subramanian, S. Karthick, A. Munusamy, Synthesis of silver nanoparticles using *Solanum trilobatum* fruits extract and its antibacterial, cytotoxic activity against human breast cancer cell line MCF 7, *Spectrochim. Acta A Mol. Biomol. Spectrosc.* 140 (2015) 223–228.
- [10] S. Rajeshkumar, Synthesis of silver nanoparticles using fresh bark of *Pongamia pinnata* and characterization of its antibacterial activity against gram positive and gram negative pathogens, *Resour. Efficient Technol.* 2 (2016) 30–35.
- [11] P.K. Khanna, K. Deepti, K.B. Rupinder, Synthesis and characterization of myristic acid capped silver nanoparticles, *J. Nanopart. Res.* 10 (2008) 1059–1062.
- [12] S. Pattanayak, M.R. Mollick, D. Maity, S. Chakraborty, S.K. Dash, S. Chattopadhyay, S. Roy, D. Chattopadhyay, M. Chakraborty, *Butea monosperma* bark extract mediated green synthesis of silver nanoparticles: characterization and biomedical applications, *J. Saudi Chem. Soc.* 21 (2017) 673–684.
- [13] A. Sasikala, M.L. Rao, N. Savithramma, T.N.V.K.V. Prasad, Synthesis of silver nanoparticles from stem bark of *Cochlospermum religiosum* (L.) Alston: an important medicinal plant and evaluation of their antimicrobial efficacy, *Appl. Nanosci.* 5 (2015) 827–835.
- [14] J. Ma, J. Zhang, Z. Xiong, Y. Yong, X.S. Zhao, Preparation, characterization and antibacterial properties of silver-modified graphene oxide, *J. Mater. Chem.* 21 (2011) 3350–3352.
- [15] V.A. Kumar, T. Uchida, T. Mizuki, Y. Nakajima, Y. Katsube, T. Hanajiri, T. Maekawa, Synthesis of nanoparticles composed of silver and silver chloride for a plasmonic photocatalyst using an extract from a weed *Solidago altissima* (goldenrod), *Adv. Nat. Sci. Nanosci. Nanotechnol.* 7 (2016), 015002.
- [16] K. Lawrence, J.D. Watkins, T.D. James, J.M. Taylor, S.D. Bull, G.W. Nelson, J.S. Foord, Y.T. Long, F. Marken, Diocetylamine-sulfonamide-modified carbon nanoparticles as high surface area substrates for coenzyme Q10-lipid electrochemistry, *Electroanalysis* 5 (2012) 1003–1010, <https://doi.org/10.1002/elan.201200121>.
- [17] D. Nayak, S. Ashe, P.R. Rauta, M. Kumari, B. Nayak, Bark extract mediated green synthesis of silver nanoparticles: evaluation of antimicrobial activity and antiproliferative response against osteosarcoma, *Mater. Sci. Eng. C* 58 (2016) 44–52.
- [18] M.J. Masarudin, S.M. Cutts, B.J. Evison, D.R. Phillips, P.J. Pigram, Factors determining the stability, size distribution, and cellular accumulation of small, monodisperse chitosan nanoparticles as candidate vectors for anticancer drug delivery: application to the passive encapsulation of [ 14 C ] -doxorubicin, *Nanotechnol. Sci. Appl.* 8 (2015) 67–80.

- [19] B. Reidy, A. Haase, A. Luch, K.A. Dawson, I. Lynch, Mechanisms of silver nanoparticle release, transformation and toxicity: a critical review of current knowledge and recommendations for future studies and applications, *Materials* 6 (2013) 2295–2350.
- [20] K. Chamakura, R. Perez-ballesterro, Z. Luo, S. Bashir, J. Liu, Comparison of bactericidal activities of silver nanoparticles with common chemical disinfectants, *Colloid. Surf. B Biointerfaces* 84 (2011) 88–96.
- [21] S. Bashir, K. Chamakura, R. Perez-Ballesterro, Z. Luo, J. Liu, Mechanism of silver nanoparticles as a disinfectant, *Int. J. Green Nanotechnol.* 3 (2011) 37–41.
- [22] S. Prabhu, E.K. Poulouse, Silver nanoparticles: mechanism of antimicrobial action, synthesis, medical applications and toxicity effects, *Int. Nano Lett.* 2 (2012) 32.
- [23] K. Logaranjan, A.J. Raiza, S.C. Gopinath, Y. Chen, K. Pandian, Shape and size Controlled synthesis of silver nanoparticles using *Aloe vera* plant extract and their antimicrobial activity, *Nanoscale Res. Lett.* 11 (2016) 520.
- [24] P. Velusamy, C.H. Su, G. Venkat Kumar, S. Adhikary, K. Pandian, S.C.B. Gopinath, Y. Chen, P. Anbu, Biopolymers regulate silver nanoparticle under microwave irradiation for effective antibacterial and antibiofilm activities, *PLoS One* 11 (2016), e0157612.
- [25] A.M. Elgorban, A.N. Al-rahmah, S.R. Sayed, A. Hirad, A.A.F. Mostafa, A.H. Bahkali, Antimicrobial activity and green synthesis of silver nanoparticles using *Trichoderma viride*, *Biotechnol. Biotechnol. Equip.* 30 (2016) 299–304.
- [26] M.P. Maigorzata, K.J. Depciuch, Green synthesis and antibacterial effects of aqueous colloidal solutions of silver nanoparticles using camomile terpenoids as a combined reducing and capping agent, *Bioproc. Biosyst. Eng.* 39 (2016) 1213–1223.
- [27] U. Kurtan, A. Güner, Md Amir, A. Baykal, Enhanced antibacterial performance of Fe<sub>3</sub>O<sub>4</sub>-Ag and MnFe<sub>2</sub>O<sub>4</sub>-Ag nanocomposites, *Bulletin Mat. Sci.* 140 (2017) 147–155.
- [28] Y. Junejo, A. Güner, A. Baykal, Synthesis and characterization of amoxicillin derived silver nanoparticles: its catalytic effect on degradation of some pharmaceutical antibiotics, *Appl. Surf. Sci.* 317 (2014) 914–922.
- [29] S. Ramanathan, S.C.B. Gopinath, Potentials in synthesizing nanostructured silver nanoparticles, *Microsyst. Technol.* 23 (2017) 4345–4357.
- [30] M.E. Foo, P. Anbu, S.C.B. Gopinath, T. LakshmiPriya, C.G. Lee, H.S. Yun, M.N.A. Uda, A.R.W. Yaakub, Antimicrobial activity of functionalized single-walled carbon nanotube with herbal extract of Hemptedu bumi. *Surf. Interface Anal.* (doi: 10.1002/sia.6375).
- [31] S. Anniebell, S.C.B. Gopinath, Polymer conjugated gold nanoparticles in biomedical applications, *Curr. Med. Chem.* 25 (2018) 1–13.
- [32] K.H. Suk, S.C.B. Gopinath, P. Anbu, T. LakshmiPriya, Cow urine encapsulated cellulose nanoparticles for effective inhibition of pathogens. *Powder Technol.* (doi.org/10.1016/j.powtec.2018.01.010).
- [33] K.H. Suk, S.C.B. Gopinath, Drug encapsulated nanoparticles for treating targeted cells, *Curr. Med. Chem.* 24 (2017) 3310–3321.
- [34] M.E. Foo, S.C.B. Gopinath, Feasibility of graphene in biomedical applications, *Biomed. Pharmacother.* 94 (2017) 354–361.